Proton and hydrogen transport through two-dimensional monolayers

2016 2D Mater. 3 025004

(http://iopscience.iop.org/2053-1583/3/2/025004)

2D Materials

RECEIVED
11 December 2015

REVISED
28 January 2016

ACCEPTED FOR PUBLICATION
25 February 2016

PUBLISHED
30 March 2016

PAPER

Proton and hydrogen transport through two-dimensional monolayers

Max Seel and Ravindra Pandey

Department of Physics, Michigan Technological University, Houghton MI 49931, USA

E-mail: seel@mtu.edu

Keywords: proton transport, graphene, h-BN, phosphorene, silicene, MoS_2, hydrogen storage

Abstract

Diffusion of protons and hydrogen atoms in representative two-dimensional materials is investigated. Specifically, density functional calculations were performed on graphene, hexagonal boron nitride (h-BN), phosphorene, silicene, and molybdenum disulfide (MoS_2) monolayers to study the surface interaction and penetration barriers for protons and hydrogen atoms employing finite cluster models. The calculated barrier heights correlate approximately with the size of the opening formed by the three-fold open sites in the monolayers considered. They range from 1.56 eV (proton) and 4.61 eV (H) for graphene to 0.12 eV (proton) and 0.20 eV (H) for silicene. The results indicate that only graphene and h-BN monolayers have the potential for membranes with high selective permeability. The MoS_2 monolayer behaves differently: protons and H atoms become trapped between the outer *S* layers in the Mo plane in a well with a depth of 1.56 eV (proton) and 1.5 eV (H atom), possibly explaining why no proton transport was detected, suggesting MoS_2 as a hydrogen storage material instead. For graphene and h-BN, off-center proton penetration reduces the barrier to 1.38 eV for graphene and 0.11 eV for h-BN. Furthermore, Pt acting as a substrate was found to have a negligible effect on the barrier height. In defective graphene, the smallest barrier for proton diffusion (1.05 eV) is found for an oxygen-terminated defect. Therefore, it seems more likely that thermal protons can penetrate a monolayer of h-BN but not graphene and defects are necessary to facilitate the proton transport in graphene.

1. Introduction

Recently, monolayers of graphene and hexagonal boron nitride (h-BN) have been found permeable to thermal protons, whereas no proton transport was detected for a molybdenum disulfide (MoS_2) monolayer [1]. The overall theoretical understanding is still somewhat limited and the high interest in various hydrogen-based technologies and other applications warrants a systematic theoretical treatment of the interaction of proton and hydrogen atoms with various monolayer materials. In addition to graphene, h-BN and MoS_2 monolayers, other single-layer sheets have become candidates of interest in the quest to find new metallic, semiconducting, and insulating two-dimensional (2D) materials for possible applications in hydrogen fuel cells, novel batteries, solar cells, transistors, LED materials and sensors [2]: silicene, a one-layer-thick sheet of Si atoms arranged in a puckered honeycomb shape [3] resembling the Si(111) surface, phosphorene, a single layer of black phosphorus [4] and blue phosphorene, an allotrope of phosphorene in puckered form [5].

The most widely studied process is the interaction of hydrogen atoms and protons with graphene [6–13]. The calculated barriers for hydrogen penetration through the center of a hexagonal ring vary considerably with the method being used, from 15 eV obtained using classical molecular dynamics calculations [6] to 2.86 eV [9] employing density functional theory (DFT) with a Perdew–Wang 91 (PW91) gradient-corrected functional [14]. A simulation using the nudged elastic-band (NEB) method within DFT yielded a 4.2 eV barrier for H penetration in graphene [10]. Near surface binding energy curves for hydrogen on benzene C_6H_6, coronene $C_{24}H_{12}$, and graphene show a physisorption minimum of 0.005 eV–0.107 eV, depending on the system and method used [11].

Similarly, calculated barriers for proton penetration in graphene are 1.17 eV [12] (using projector-augmented plane waves (PAW)), 2.21 eV and 1.41 eV [9] (NEB and PW91 potential energies), 1.26 eV [1] (climbing-image (CI) NEB density functional calculation), between 1.3 and 1.4 eV [1] (using *ab initio*

molecular dynamics simulation), and ~0.6 eV if the effect of Pt on proton transport is included in the CI NEB calculation [1]. Computer simulation of aqueous proton transfer across nanoscale holes and defects in graphene reveal low energy barriers of 0.61–0.75 eV but 3.9 eV without any vacancies in the 2d lattice [13].

The calculations for the proton/graphene system were extended to a monolayer of h-BN [1]. The resulting barrier was computed to be 0.68 eV. No calculations were made for MoS_2. The absence of proton transport through MoS_2 monolayers was explained with the observed higher electron density in the hexagons of the MoS_2 monolayer [1].

In this paper we report the results of calculations for proton and hydrogen transport through these three 2D materials and extend the study to phosphorene and silicene. Note that for all systems the same method is applied to calculate the interaction potential curve as a function of distance of the proton or hydrogen atom from the center of the open site of graphene, h-BN, phosphorene, silicene, and MoS_2 monolayers. A cluster model approach is used, i.e., the 2D sheet is represented by a finite number of atoms. This approach has been employed since a long time to use accurate *ab initio* methods of quantum chemistry for a quantitative description and detailed understanding of the interaction between atoms and molecules and a solid surface. An early example is the study of the adsorption and surface penetration of atomic hydrogen at the open site of Si(111) [15] which resembles the hydrogen/silicene system. Barrier heights are calculated and compared using the differential heights of the total energy profiles.

The calculations show that the barrier heights correlate approximately with the size of the opening formed by the six-fold or three-fold open sites of the various monolayers. The only exception is found for the MoS_2 sheet which can trap protons and hydrogen atoms in the Mo plane between the outer S layers. Additional calculations for graphene and hBN are performed since the understanding of thermal proton transfer across a single layer of graphene is still limited, especially whether defects are necessary [13] or not [1].

2. Method and computational details

While most studies mentioned in the introduction employed methods with periodic boundary conditions, here the cluster model approach is used which focuses on the local nature of the interaction. While there is no *a priori* reason that one approach is more appropriate or better, one method might offer advantages over the other depending on the problem at hand. The cluster approach when properly handled and tested has the advantage that the whole toolkit of modern quantum chemistry and many comparisons to experimental data are available to give reasonable estimates about the quality of the results.

The choice of cluster size is an important consideration. Before the $X_{54}H_{18}$ clusters pictured in figure 1 were chosen some exploratory calculations were performed on the smaller $C_{24}H_{12}$ and $Mo_{12}S_{24}$ cluster with only one band of neighboring hexagons around the central hexagon. The smaller cluster models gave already the same qualitative results for barrier (graphene) and well depth (MoS_2) with a 10% difference (15% for MoS_2) in absolute values. A calculation for the barrier height for H penetration on graphene employing a $C_{96}H_{24}$ cluster (adding another band of benzene hexagons to the $C_{54}H_{18}$ cluster shown in figure 1(a) to have three neighbors around the center benzene ring) yielded a barrier height of 4.62 eV, virtually identical with the result for $C_{54}H_{18}$ (4.61 eV). Therefore the chosen cluster size should be appropriate and sufficient to study the trend for the various 2D materials investigated in this paper.

All calculations were performed with GAUSSIAN09 [16] using DFT with Becke's three-parameter hybrid functional B3LYP [17] with non-local correlation provided by the Lee, Yang, and Parr (LYP) expression [18]. For all systems except MoS_2 the GAUSSIAN09 6-31(d,p) basis sets were used. The B3LYP 6-31(d,p) level of theory has eVolved as a standard for a reasonable balance between accuracy and computer time for larger system when compared to available experimental data. For the MoS_2 study, the effective core potential (ECP) LANL2DZ basis [19] was employed. For *S*, the $3s^2\ 3p^4$ electrons represent the active valence space, for Mo, not only the $4s^1 4d^5$ electrons but also the $4s^2 4p^6$ electrons are included in the active valence space to accurately describe the chemical bonding.

The cluster models for the calculation of the potential curves of the interaction of a proton or hydrogen atom with the various 2D monolayers are shown in figures 1(a)–(f). For example, $C_{54}H_{18}$ depicted in figure 1(a) is a circular cluster in which the central hexagon has two neighboring bands of benzene rings to minimize effectively edge effects. The interaction potential curve is calculated as a function of the vertical distance *D* from the center of the central hexagon. Terminating hydrogens are used to embed the cluster. They are placed so that each boundary carbon atom has the correct number of nearest neighbors and sp^2 hybridization. This embedding procedure has been used successfully in many cluster model studies. The cluster geometries have been optimized with the 6-31basis (without polarization functions), mainly to optimize the termination with hydrogen atoms and to ensure that the model clusters are in an equilibrium geometry and the virial theorem $-V/T = 2$ is fulfilled (in the case of the ECP calculations with the LANL2DZ basis set, the virial theorem no longer applies). Similar descriptions cover the other 2D monolayer clusters $B_{27}N_{27}H_{18}$, $P_{54}H_{18}$ and $Si_{54}H_{18}$. Not unexpectedly, the $Mo_{27}S_{54}$ cluster with 27 metal Mo atoms with open d

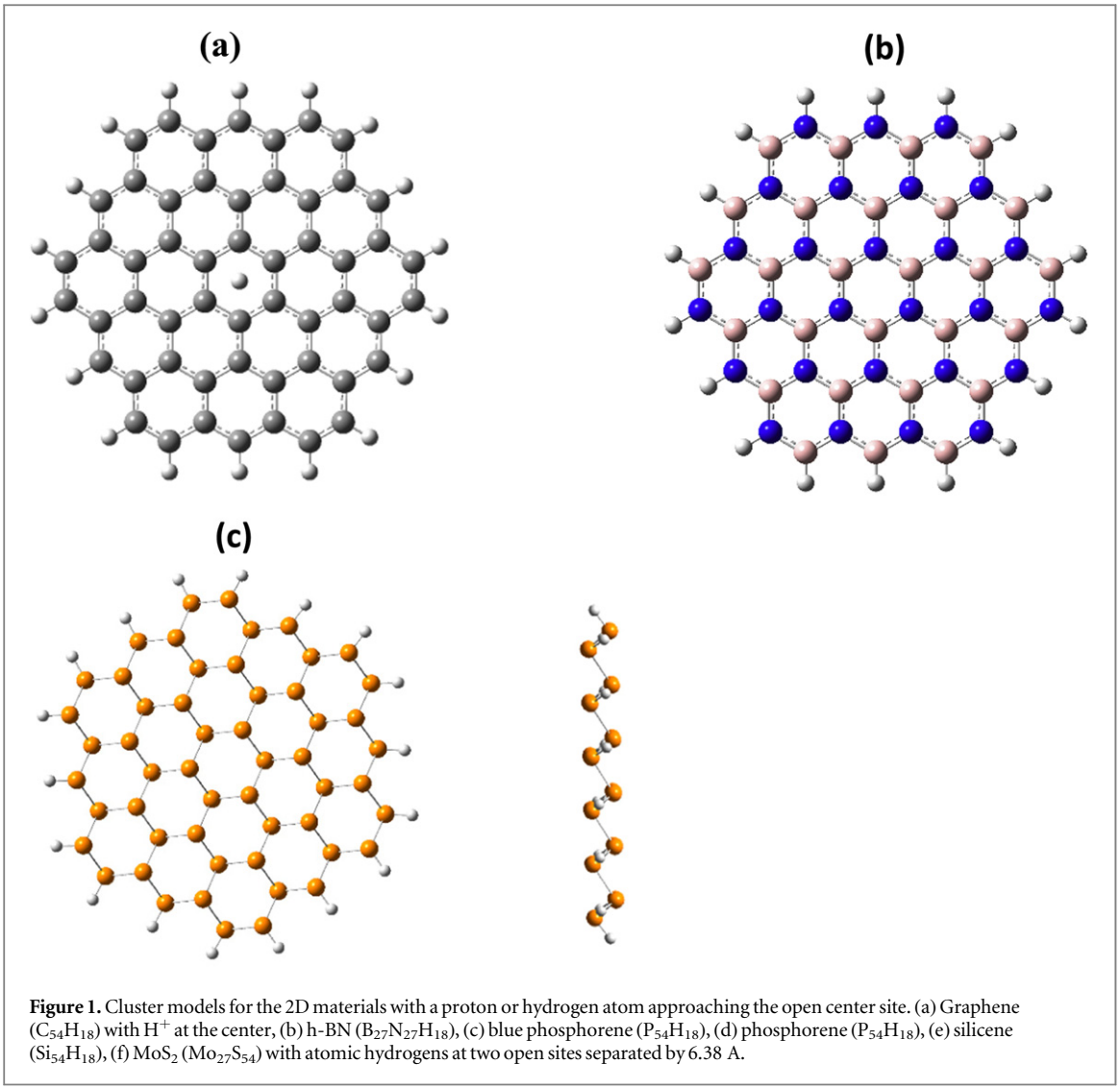

Figure 1. Cluster models for the 2D materials with a proton or hydrogen atom approaching the open center site. (a) Graphene ($C_{54}H_{18}$) with H^+ at the center, (b) h-BN ($B_{27}N_{27}H_{18}$), (c) blue phosphorene ($P_{54}H_{18}$), (d) phosphorene ($P_{54}H_{18}$), (e) silicene ($Si_{54}H_{18}$), (f) MoS_2 ($Mo_{27}S_{54}$) with atomic hydrogens at two open sites separated by 6.38 A.

shells provides different challenges. They are addressed below in more detail.

For the bare monolayer ML, spin-restricted (unpolarized) singlet calculations are performed. When a proton is added, the system (ML + H^+) is still a singlet with charge +1. For larger distances of the proton from the monolayer, the lower energy state is (ML^+ + H): it costs less energy to remove an electron from the monolayer ML than from the hydrogen atom. The energy minimization converges to this limit which is correctly described by a triplet state. This is illustrated in detail for the proton/graphene system where the triplet state becomes lower at about 1.5 A above the surface. Therefore, the proton calculations describe accurately the near-surface interaction, but they cannot be expected to describe properly the dissociation of ML—H^+ for larger distances D. For that reason, as in earlier calculations (see [1] for graphene and h-BN), the penetration barriers are calculated using the differential height of the *total energy* profile near the surface not the *binding energy* $\Delta E(D) = E(\mathrm{ML} + \mathrm{H}^+, D) - E(\mathrm{ML}) - E(\mathrm{H}^+)$.

For the ML/H systems (except for MoS_2), spin-unrestricted doublet calculations are performed. The results of the calculations are found to be free of spin contaminations, i.e., $\langle S^2 \rangle = s(s+1) = 0.75$ is obtained with high accuracy, and all calculations exhibit proper dissociation behavior $\Delta E(D) -> 0$ for $D -> \infty$. The penetration barriers are therefore calculated from the binding energy curve $\Delta E(D) = E(\mathrm{ML} + \mathrm{H}, D) - E(\mathrm{ML}) - E(\mathrm{H})$.

Finite clusters calculations with many metal atoms as in a $Mo_{27}S_{54}$ cluster pose a challenge due to the many possible electronic states and spin multiplicities. The electronic structure of a single MoS_2 monolayer as calculated in local DFT [20] and with the PAW method [21] has been confirmed to be a direct band gap semiconductor with a gap of 1.79 eV [20] (1.59 eV [21]). Therefore, a finite cluster model describing the (infinite) monolayer should be a zero spin singlet state. Earlier calculations for MoS_2 clusters indicate [22] that in smaller clusters the spin triplet is more stable than the singlet (the ground state of MoS_2, the smallest molecular model for the MoS_2 catalyst, is a quintet [23]) but that for larger clusters the singlet is nearly

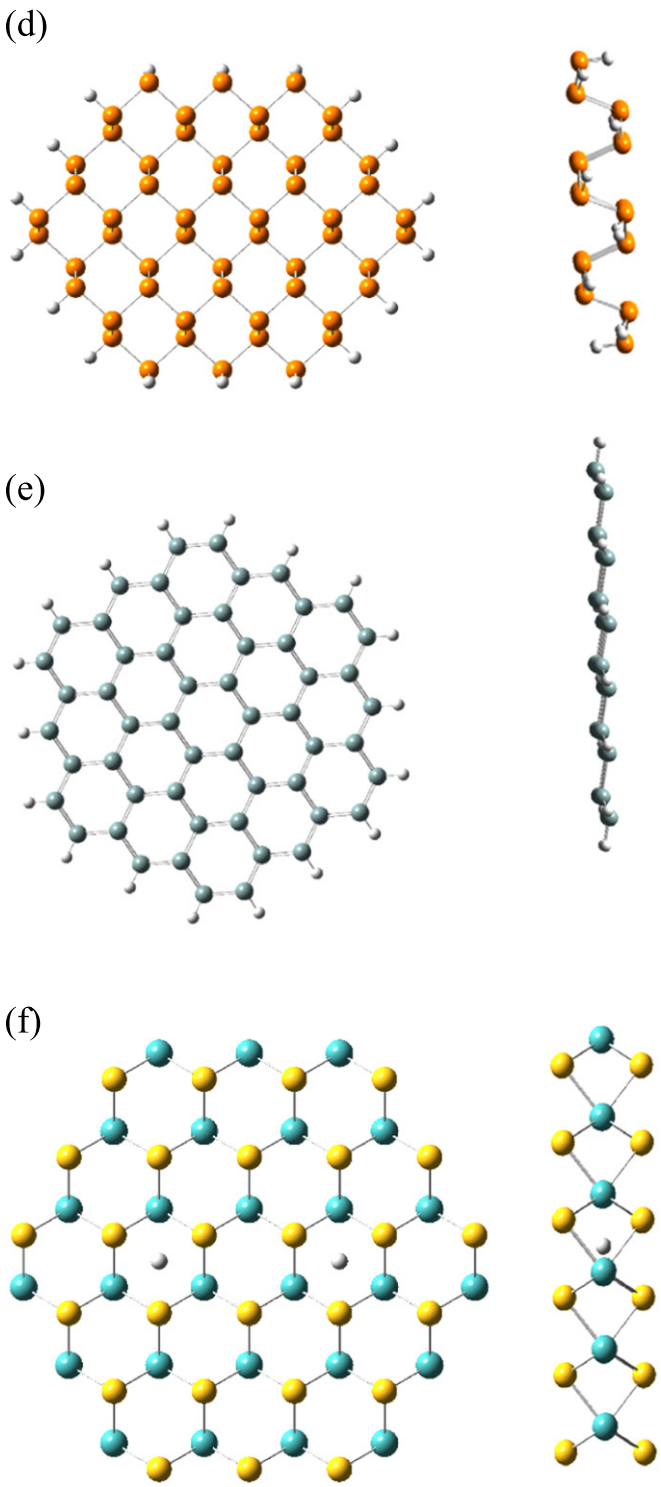

Figure 1. (Continued.)

equally stable as the triplet, reflecting the fact that the infinite MoS_2 crystal and sheet are semiconducting and not metallic. On triangular-shaped MoS_2 nanosheets, edge effects have been studied [24]. Depending on stoichiometric ratios, spin-polarized calculations show that the magnetization depends on the specific nature of the Mo and S edges, but that for quite a few configurations, the singlet unpolarized state is the ground state. In a DFT cluster model calculation for the H_2 dissociation on MoS_2, terminating hydrogen atoms were used [25] to give the edge Mo and S atoms the proper coordination and to keep the Mo/S ratio equal to 2.

For all these reasons, the proton interaction with MoS_2 is first studied on a smaller $Mo_{12}S_{24}$ cluster with and without terminating hydrogen atoms to make

Table 1. Penetration barriers in eV through open site as calculated from the differential height of the energy profiles near the surface. For MoS_2 the value indicates the depth of the well.

	Graphene	h-BN	Blue phosphorene	Phosphorene	Silicene	MoS_2
Proton (H^+) (eV)	1.56	0.91	0.64	0.48	0.12	1.56
Hydrogen atom (eV)	4.61	6.38	0.86	0.60	0.20	1.50
Hexagon Radius (A)	1.42	1.45	2.15	2.15[a]	2.28	1.84

[a] Distance from center to nearest P atom.

sure that the qualitative features of the proton interaction in the center of the cluster do not depend on the embedding or termination of the cluster. As before, singlet (unpolarized) calculations are performed for the proton/MoS_2 interaction potential. When higher spin states were tested, large spin contaminations were found. Therefore, instead of performing spin-unrestricted calculations for the doublet state of the H/MoS_2 system, *two* hydrogen atoms, separated by a distance of 6.38 A, approaching two open sites of the MoS_2 monolayer as depicted in figure 1(f) were studied as a ($Mo_{27}S_{54}$—H H) singlet state. The binding energy curve is calculated as before as $\Delta E(D) = E(\mathrm{ML} + 2\ \mathrm{H}, D) - E(\mathrm{ML}) - 2\,E(H)$. For large D away from the surface, $\Delta E(D)$ will not become zero, but a dissociation error $e = E(2\ \mathrm{H}) - 2\,E(\mathrm{H})$ can be expected, indicative of the improper dissociation of 2 H atoms (or, generally, 2 open shell atoms) in DFT [26]: as shown below, in B3LYP with the LANL2DZ basis, for 2 H atoms separated by 6.38 A, this error is 3 eV.

3. Results and discussion

3.1. Gas-phase penetration barriers

First, the results for the energy profile curves for proton and hydrogen atoms penetrating the various monolayers direct through the center of the central open site are summarized to establish a baseline for comparison of the different 2D materials. In a subsequent section 3.2. more detailed geometry and energy calculations including the presence of Pt atoms and, in section 3.3, the effect of a quad-vacancy and a solvent are discussed in relation to the recent experimental results for graphene and h-BN [1, 13] to shed some light on the still not fully understood proton transfer mechanism.

Table 1 summarizes the idealized gas-phase penetration barriers (in eV) for the various 2D sheets. The potential curves from which the barriers are calculated are shown in figures 2(a)–(f) for protons and in figures 4(a)–(f) for hydrogens.

3.1.1. Proton barriers

As discussed before the penetration barriers are calculated from the differential height of the total energy profiles near the surface because the ($\mathrm{ML} + H^+$) calculations cannot properly describe the dissociation for larger distances from the surface. The penetration barrier as obtained from the interaction potential curve of the proton approaching the center of the central benzene ring of graphene (see figure 2(a)) is found to be 1.56 eV. This value falls within the range of earlier results discussed in the introduction and does not support thermal proton transfer through graphene. Figure 2(a) also shows the triplet state interaction potential curve (dotted line) which demonstrates that the total energy calculation for larger distances from the surface produces dissociation towards the ($C_{54}H_{18}^+ + \mathrm{H}$) system (−2069.2570 a.u.) instead of the ($C_{58}H_{18} + H^+$) system (−2068.9758 a.u.).

The barrier heights decrease from 1.57 eV for graphene to 0.91 eV for h-BN, 0.64 eV for blue-phosphorene, 0.48 eV for phosphorene, and 0.12 eV for silicene. This decrease approximately correlates with the increase of the hexagon radius or the distance from the center proton to the nearest monolayer atom: it is 1.42 A for graphene, 1.45 A for h-BN, 2.15 A for blue-phosphorene, 2.15 A for phosphorene, and 2.28 A for silicene. The thickness of the barrier correlates with the puckering (buckling) geometry of the layers (see figures 1(c) and (d)): the puckering constant δ is found to be 1.2 A for the optimized blue-phosphorene cluster, 2.2 A for phosphorene, and 0.44 A for silicene.

The 42% decrease in barrier height from graphene to h-BN is of course not just due to the 2% larger opening in h-BN but can be explained with the strong ionic character of the h-BN sheet which a Bader charge analysis [27, 28] confirmed: our calculations show a 2.17e transfer from B to N. The boron atoms of the central hexagon have a total electronic charge of 2.83 and the nitrogen atoms have 9.17e. These results are in line with an earlier experimental and theoretical study [29] which found +2.7e for the B ion and −1.9e for the N ion. The proton at $D = 0$ picks up a charge of 0.40e in the graphene case and 0.45e from h-BN. In the case of h-BN this charge facilitates some ionic interaction and bonding (see figure 3) and, ultimately, barrier reduction. As shown below this ionic interaction also leads to a further significant barrier reduction if the center geometry is allowed to relax.

The interaction potential curve for the proton (H^+) on MoS_2 looks very different from the ones discussed so far. As seen in figure 2(f) a well is found with a depth of 1.56 eV which traps the proton in the Mo layer between the two outer S layers. As discussed before, to ensure that the results are independent of the embedding procedure, the proton interaction was

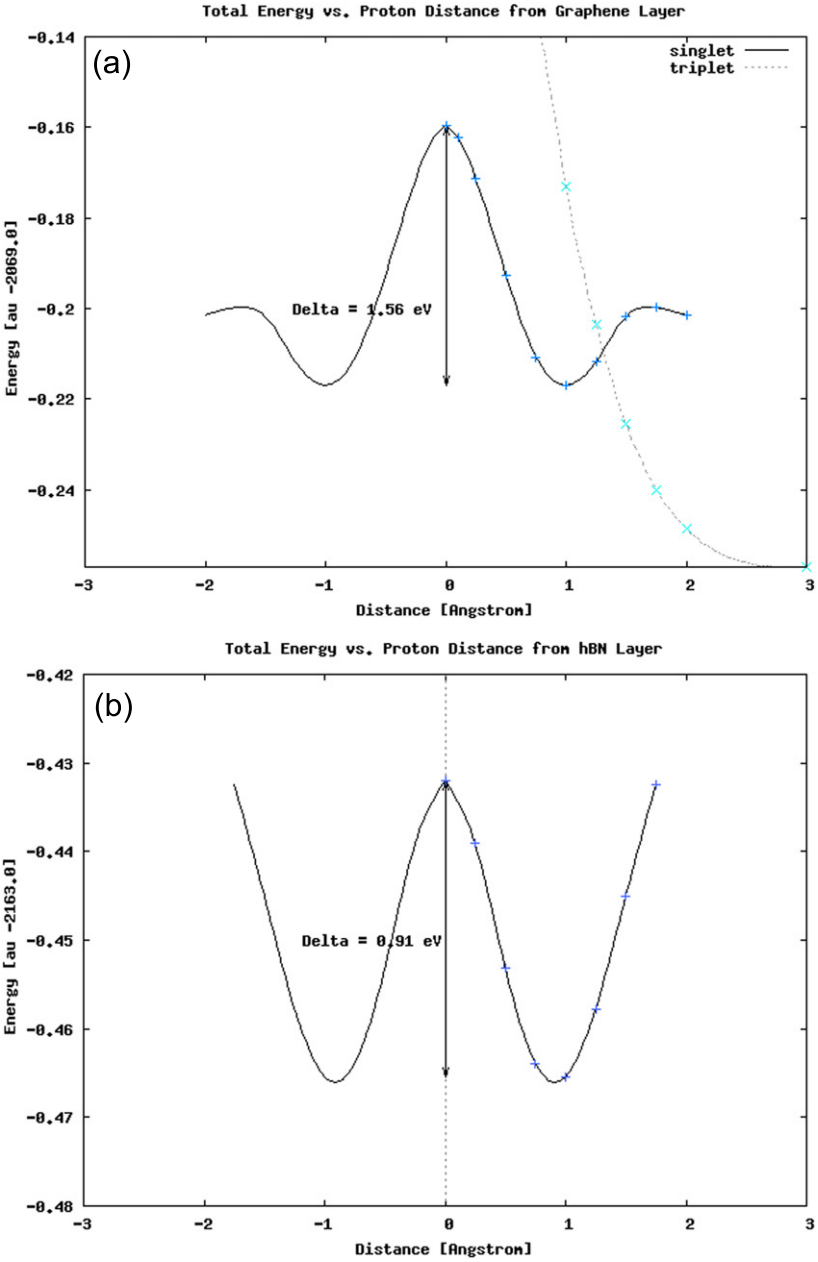

Figure 2. (a) Total energy of the ($C_{54}H_{18}$ + proton) system as function of proton (H^+) distance from the center of the central hexagonal ring of the graphene cluster. The barrier for penetration is defined by the differential height of the singlet state energy profile. The triplet state profile (dotted line) demonstrates that the total energy calculations for larger distances from the surface produce dissociation towards the ($C_{54}H_{18}^+$ + H) system (−2069.2570 a.u.) instead of the ($C_{54}H_{18}$ + H^+) system (−2068.9758 a.u.). $\Delta = 1.56$ eV. (b) Total energy versus proton distance from h-BN layer; $\Delta = 0.91$ eV. (c) Total energy versus proton distance from blue-phosphorene layer; $\Delta = 0.64$ eV. (d) Total energy versus proton distance from phosphorene layer; $\Delta = 0.48$ eV. (e) Total energy versus proton distance from silicene layer; $\Delta = 0.12$ eV. (f) Total energy versus proton distance from MoS_2 layer; $\Delta = 1.56$ eV.

also studied on a smaller $Mo_{12}S_{24}$ cluster with and without terminating hydrogen atoms. Qualitatively, the results are in both cases the same: with 24 embedding H atoms the well depth was 1.64 eV, without hydrogens 1.35 eV. The existence of a well larger than 1 eV can possibly explain why no thermal proton transport was detected through the MoS_2 monolayer [1].

3.1.2. Hydrogen barriers

In figures 4(a)–(f) the binding energy curves are shown for the interaction of a hydrogen atom with graphene, h-BN, blue-phosphorene, phosphorene, silicene, and MoS_2. The binding energy $\Delta E(D)$ is plotted as a function of the vertical distance D from the center of the central hexagon. First, it can be seen that the spin-unrestricted doublet calculations give the correct dissociation behavior $\Delta E(D) -> 0$ for $D -> \infty$. The MoS_2 case with two approaching H atoms will be discussed separately.

The largest barrier for hydrogen penetration is found for h-BN (6.38 eV), followed by graphene (4.61 eV). The materials with larger open sites have substantially smaller barriers: blue-phosphorene with

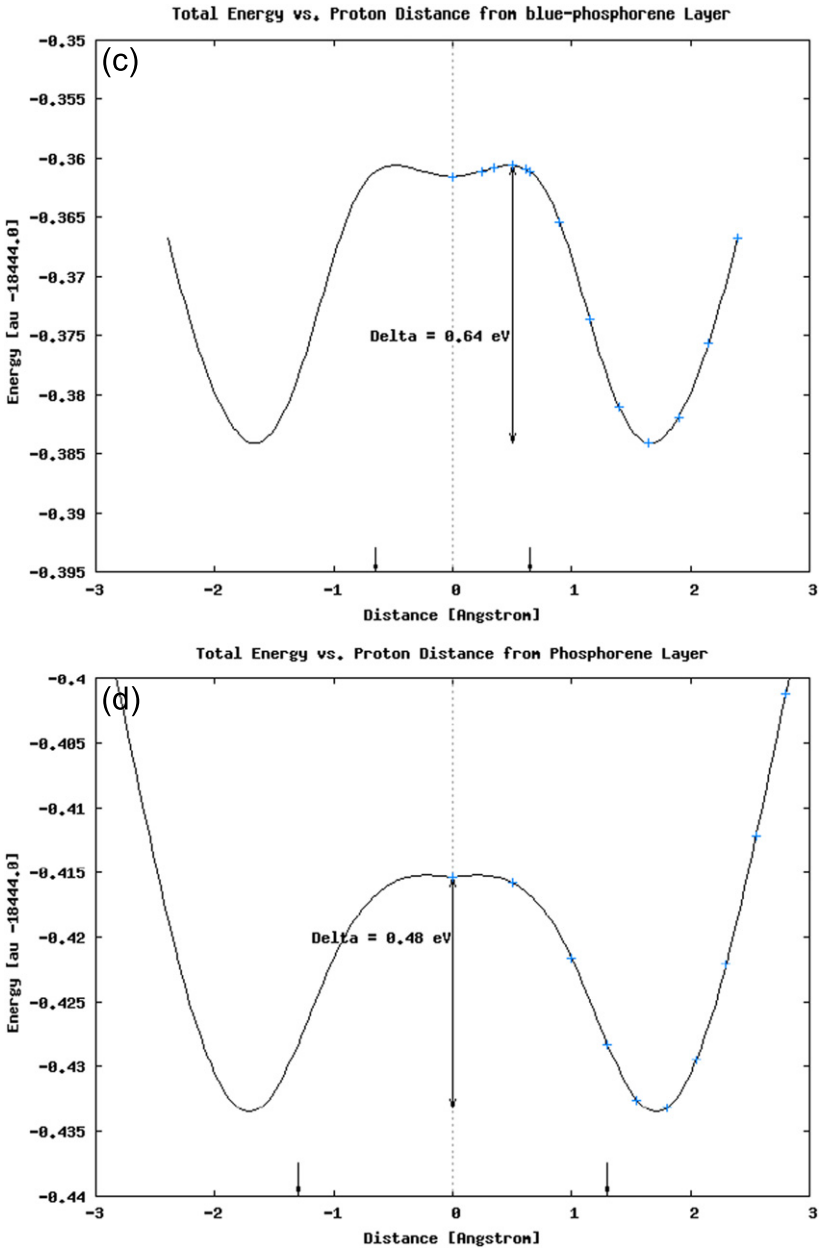

Figure 2. (Continued.)

a hexagon radius of 2.15 A has a barrier of 0.86 eV, phosphorene 0.60 eV, and silicene with a hexagon radius of 2.28 A only 0.20 eV.

The interaction curves for the last three monolayers are also different from the binding energy curves of graphene and h-BN in so far as they exhibit a clear adsorption minimum above the open site. For blue-phosphorene, an adsorption minimum of 0.41 eV is at $D = 1.65$ A which corresponds to ~1 A above the surface if the puckering of ±0.6 A is taken into account. For phosphorene the minimum of 0.16 eV is at 1.8 A, ~0.7 A above the surface (puckering ±1.1 A), and for silicene, a minimum of 0.11 eV is found at 1.22 A, ~1 A above the surface atoms (puckering ±0.22 A). The qualitative features of the hydrogen atom approaching the open site of silicene are similar to the adsorption and surface penetration at the open site of the Si(111) surface as modeled in an early cluster study [15] although the absolute values obtained with B3LYP for barrier and well for the silicene case are much smaller than the Hartree–Fock/two configurations multi-configurations self-consistent field values for Si(111).

An adsorption minimum above the open site of graphene and h-BN can also be found if dispersion is included in the calculation. As shown in figure 5, adding Grimme's empirical dispersion [30] to the B3LYP functional, one obtains a weak physisorption minimum of 0.039 eV for H 2.75 A above graphene and of 0.049 meV for H 2.5 A above h-BN. The values obtained for H on graphene are well within the bench mark data range of 0.005–0.097 eV for the adsorption

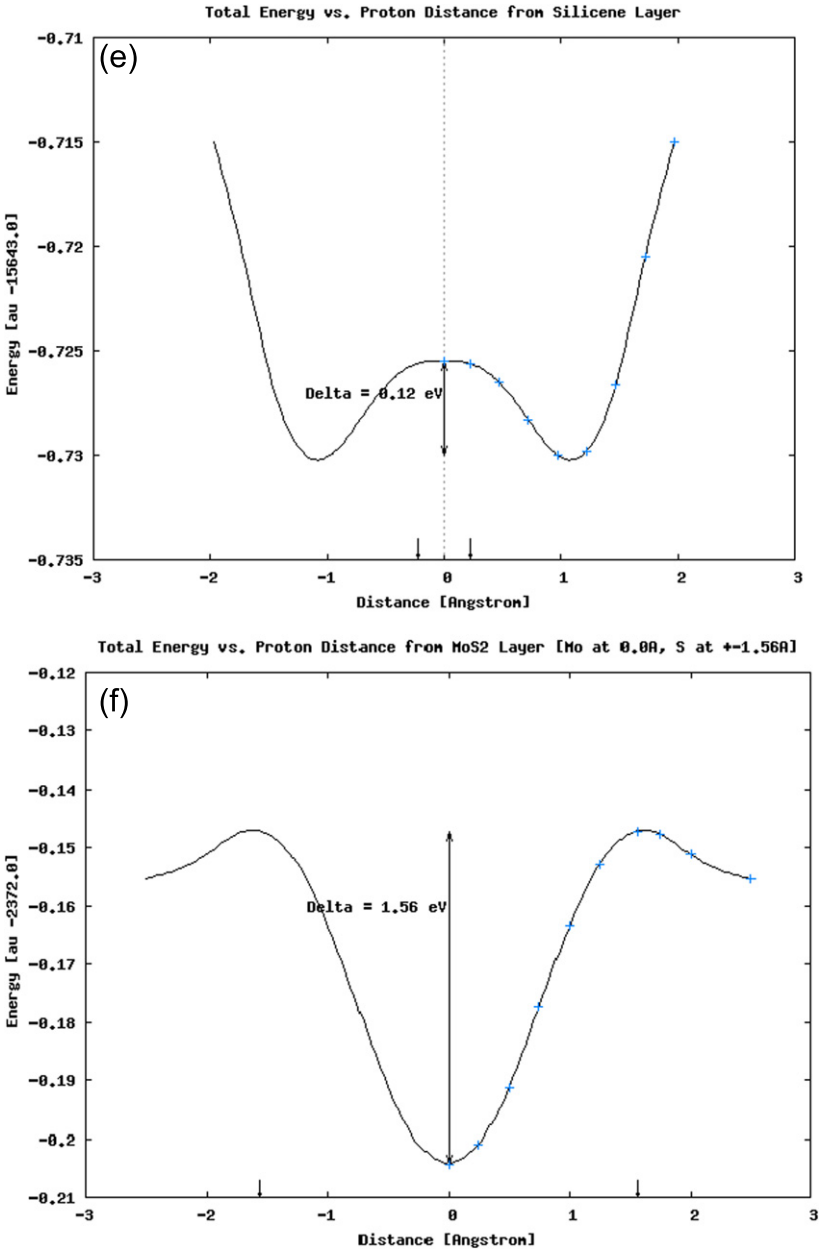

Figure 2. (Continued.)

energy and 2.5–3 A for the location of the minimum obtained with several van der Waals-density functionals [11].

It should be pointed out that the physisorption minimum found in the study of H penetration at the open site is not the preferred adsorption site. A comprehensive cluster chemisorption study would require calculations on other high-symmetry sites in addition to the open site, H on top and in the bridge position, which goes beyond the scope of the current investigation focused on transport through membrane materials. However, we can report on one adsorption result: when the appropriateness of our model was tested by comparing cluster results to other known results for H on graphene an unconstrained optimization of H on the $C_{54}H_{18}$ cluster gave as most stable position for H to be chemisorbed with a binding energy of 0.63 eV 1.12 A on top of a C atom which is pulled out from the graphene plane by 0.38 A ([9], using a periodic boundary condition method: C–H bond 1.13 A, carbon atom 0.47 A out of sheet plane).

In contrast to the proton interaction situation, the barrier for H transport through h-BN *increases* by 38% compared to graphene. A Bader charge analysis shows that in the case of graphene the hydrogen atom transfers 0.6e to the graphene sheet when it reaches the center position whereas H on hBN stays neutral with an electronic charge of 1.0e throughout the interaction. Therefore, in the case of graphene, ionic interaction between the positively charged H atom and the negatively charged graphene sheet helps reducing the barrier.

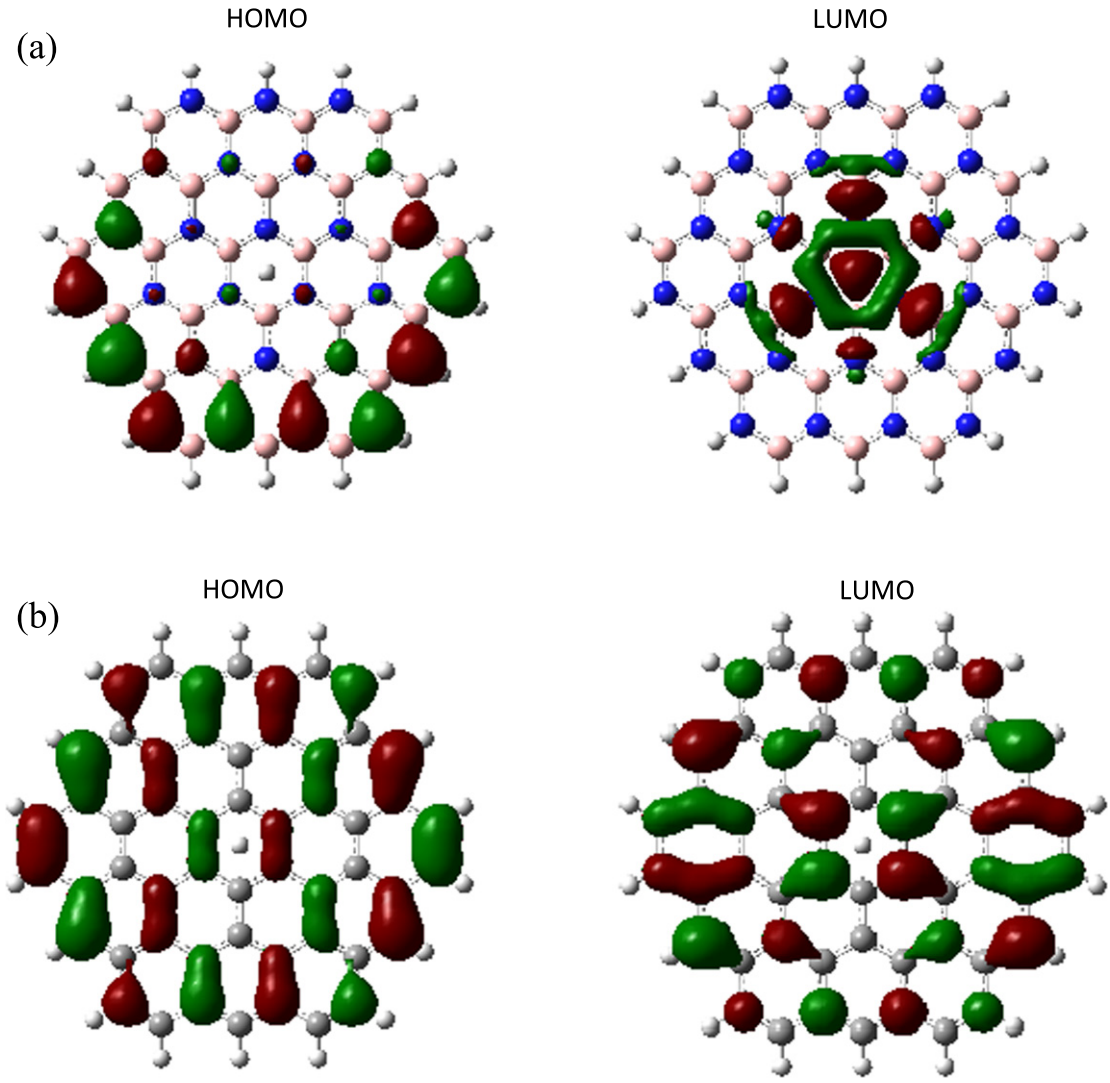

Figure 3. The HOMO and LUMO levels for hBN and graphene: (a) hBN: in addition to the strong covalent bond through the sp^2 hybridization the bonding in hBN also has a strong ionic character which allows for ionic interaction with the proton. (b) Grapheme.

The effect of this difference in charge on the hydrogen atom manifests itself also when the lattice is allowed to relax. By performing a geometry optimization for the atoms of the center hexagon and the in-plane hydrogen atom, the barrier for penetrating graphene is reduced from from 4.61 eV to 4.33 eV (6%) and the hBN barrier from 6.38 eV to 6.05 eV (5%). In the case of graphene the positively charged hydrogen atom is found slightly off-center interacting with slighly negatively charged neighboring C atoms. In the case of h-BN the neutral hydrogen atom stays 'on-center'. Compared to the barrier reduction for the proton case discussed below, the reductions are less dramatic: the hydrogen atom is simply too big to go through the open site. The ionic nature of the h-BN lattice does not help because H stays neutral.

For atomic hydrogen on MoS_2 the binding energy curve again looks different from the other monolayer/H potentials, very similar to what was already encountered for the proton transport. As discussed in more detail before in section 2, to avoid spin contaminations, the interaction curve of *two* hydrogen atoms, separated by a distance of 6.38 A as shown in figure 1(f), was calculated. As can be seen from figure 4(f), the hydrogen atoms become trapped in the plane of the Mo atoms in a well of 3.00 eV (1.5 eV per H atom). A small barrier of only 0.89 eV (0.45 eV per H atom) has to be overcome to penetrate through the outer S plane.

The explanation that the binding energy does not converge to zero for large D lies in the inability of DFT to describe properly the dissociation of two open shell atoms [26]. Figure 6(a) expands the binding energy curve for 2 H atoms with constant separation of 6.38 A for larger distances D from the MoS_2 monolayer surface. The binding energy $\Delta E(D)$ approaches 3 eV which is exactly the dissociation error for two hydrogen atoms obtained in B3LYP with the LANL2DZ basis as shown in figure 5(b) depicting the singlet and triplet interaction curves for 2 H atoms.

The results so far indicate that only graphene and h-BN monolayers have the potential for membranes with high selective permeability. For phosphorene and

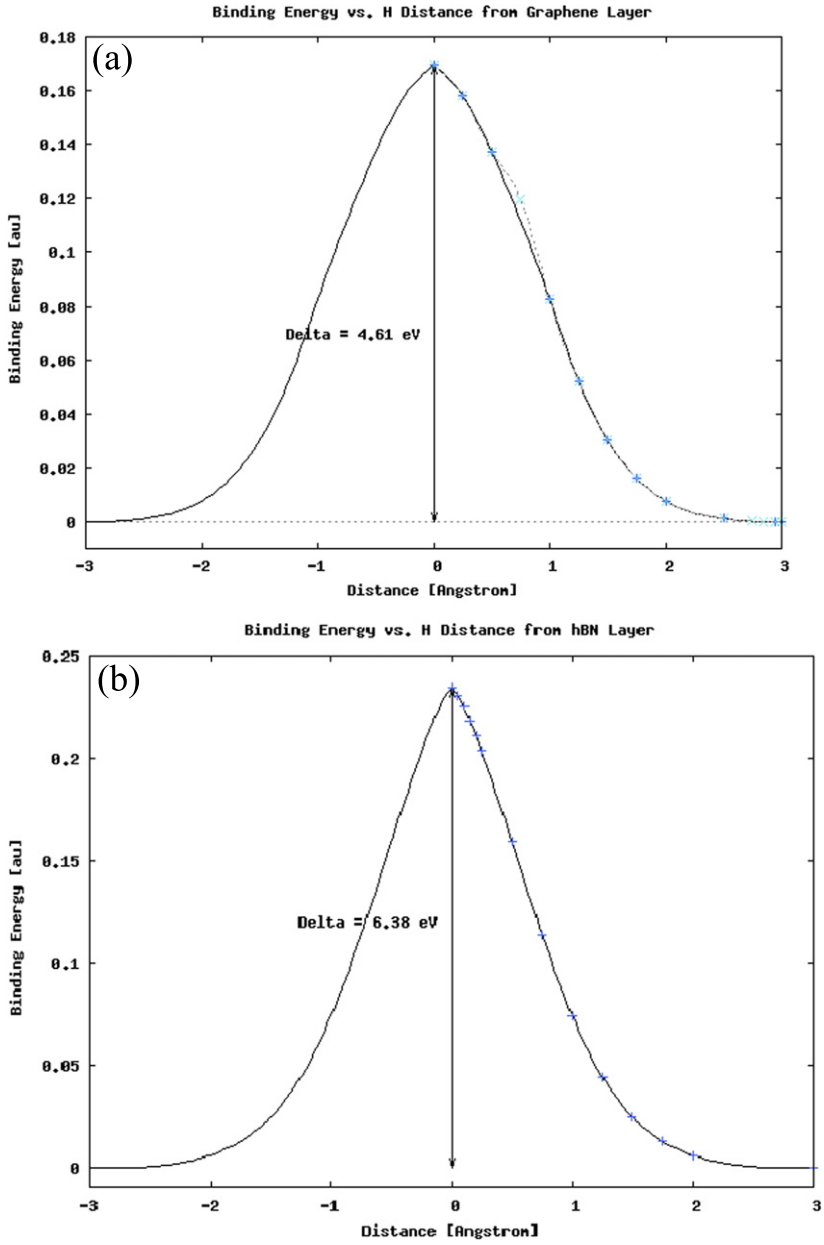

Figure 4. (a) Binding energy BE $= E(C_{54}H_{18} + H) - E(C_{58}H_{18}) - E(H)$ as function of the hydrogen distance from the center of the central hexagonal ring of the graphene cluster. BE approaches its proper value zero for infinite distances. $\Delta = 4.61$ eV. (b) Binding energy versus H Distance from h-BN Layer. $\Delta = 6.38$ eV (c) Binding energy versus H distance from blue phosphorene layer. $\Delta = 0.86$ eV. (d) Binding energy versus H distance from phosphorene layer. $\Delta = 0.60$ eV. (e) Binding Energy versus H distance from silicene layer. $\Delta = 0.20$ eV. (f) Binding energy versus distance of 2 H atoms (separated by 6.38 A) from MoS_2 Layer. Δ (Well) $= 1.50$ eV per H atom. The dissociation behavior for $D > 2.5$ A is shown in figure 6.

silicene, the gas-phase barriers for proton and hydrogen atoms, although below 1 eV, are not significantly different and therefore not effective selective membranes. Moreover, MoS_2 seems to trap both protons and hydrogens suggesting the MoS_2 monolayer as a possible hydrogen storage material instead of a membrane.

3.2. Reduction of proton penetration barrier for graphene and h-BN

In our cluster models, reduction of the proton gas-phase penetration barrier can be achieved if some system relaxation is taken into account. By allowing the atoms of the center hexagon and the in-plane proton to relax in a new geometry optimization (see figure 7), the barrier for penetrating graphene (defined as the difference of the energy minimum at ~1 A and the new value obtained for the optimized geometry) is reduced from 1.56 eV to 1.38 eV. Due to the strong ionic interaction of the proton with the boron and nitrogen ions in h-BN, a stronger distortion and a larger off-center position of the proton (see figure 7(b)) results in a substantial reduction of the h-BN barrier from 0.91 eV to 0.11 eV. In the case of graphene, the resulting off-center position of the

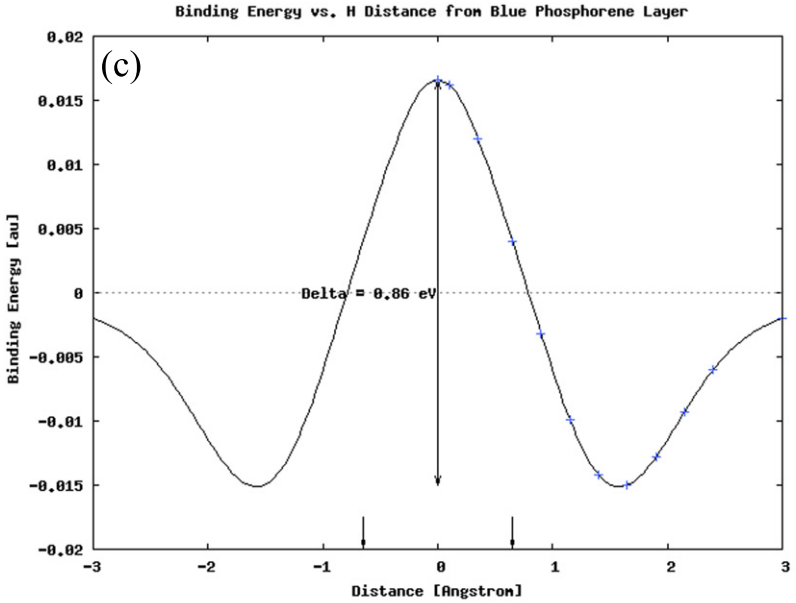

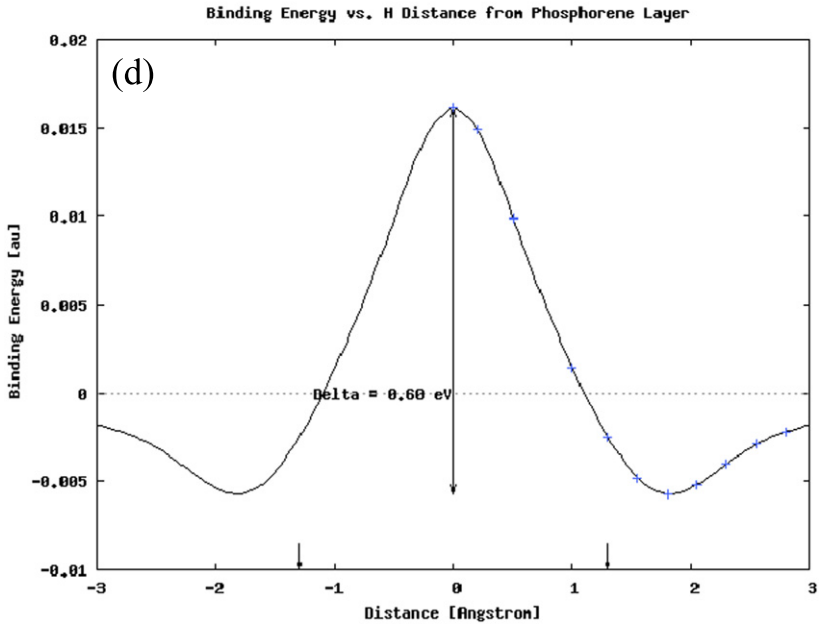

Figure 4. (Continued.)

proton due to geometry relaxation has been described before [5].

Next, the effect of Pt on the proton transport through graphene is modeled. In [1], a significant reduction of the CI-NEB barrier from 1.26 eV to ~0.6 eV was reported when 4 Pt atoms were placed at a fixed distance of 4 A from the graphene membrane. We tried to replicate the situation in our cluster model by placing 4 Pt atoms in a square arrangement with side length 2.51 A 4 A from the graphene cluster at the other side of the approaching proton as shown in figure 8. For Pt the ECP basis LANL2DZ [19] was employed and the calculations for the barrier height were repeated at the potential minimum (proton distance $D = 1$ A) and maximum ($D = 0$ for the proton being in the graphene plane). A barrier height of 1.55 eV was obtained, basically the same as without Pt (1.56 eV). Rotating the square arrangement of the 4 Pt atoms by 45° did not make any significant difference and resulted in a height of 1.53 eV. The calculations were repeated for the relaxed off-center geometry described above. Again, the presence of the 4 Pt atoms did not affect the barrier heights: the results were 1.38 and 1.37 eV.

More geometric arrangements of the 4 Pt atoms were studied on a smaller $C_{24}H_{12}$ cluster (no second neighbor benzene rings), without any different results. Finally, the calculation was performed in the presence of water to see whether a solvent has any measurable effect. The polarizable continuum model (PCM) [31] as implemented in GAUSSIAN 09 [16] was used. The program computes the energy in solution by making the solvent reaction field self-consistent with the solute electrostatic

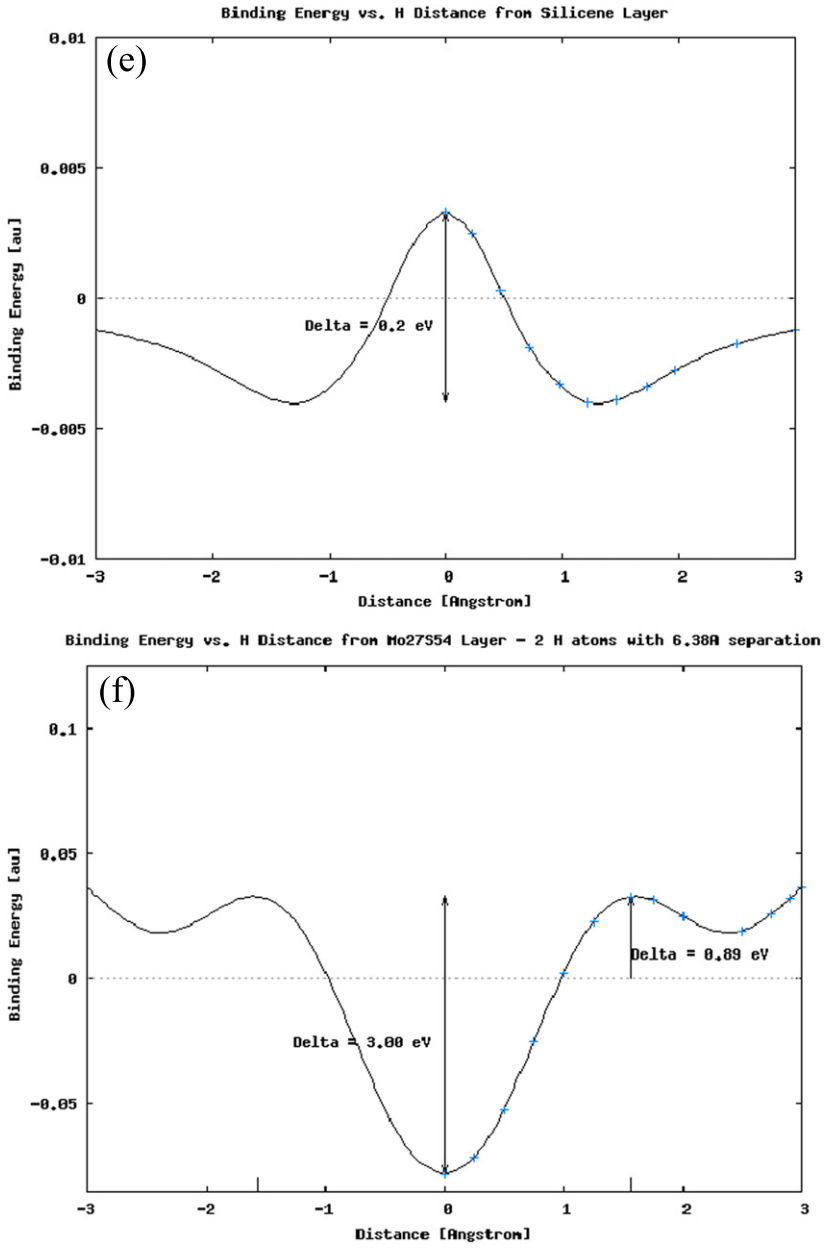

Figure 4. (Continued.)

potential which is generated from the computed electron density [16]. For water, a dielectric constant $\varepsilon = 78.35$ was used. For the smaller cluster in the presence of 4 Pt atoms, a gas-phase proton penetration barrier of 1.39 eV was obtained (1.40 eV without Pt). The presence of the solvent *increased* this barrier to 1.46 eV, the increase explained by the hydrophobic nature of graphene. It follows that the calculated gas-phase and aqueous barriers of ~1.4 eV are all too high to permit proton transfer through pristine graphene. The presence of Pt atoms had no significant effect on these barriers.

3.3. Gas-phase and aqueous penetration barriers for a four-carbon defect site

In [13] the proton transfer through carbon atom vacancy sites was studied in detail, especially for the aqueous transfer through a quad-vacancy site where the six resulting unsaturated carbon atoms are either terminated with three oxygen atoms or with six OH hydroxyl groups. It was shown that the latter provides a hydrogen-bonding network conducive to proton shuttling through the defect site resulting in the lowest calculated barrier of 0.68 eV (performing NEB periodic DFT calculations using the Vienna *ab initio* simulation package (VASP) [32]) and 0.61 eV (using reactive force field molecular dynamics simulations). This path is beyond the current static cluster model, but the 3 O-capped defect can be modeled within our approach by using a water molecule carrying a proton as a H_3O^+ hydronium ion near to the defect site and then following the proton path through the center of the oxygen-terminated defect. The findings can be

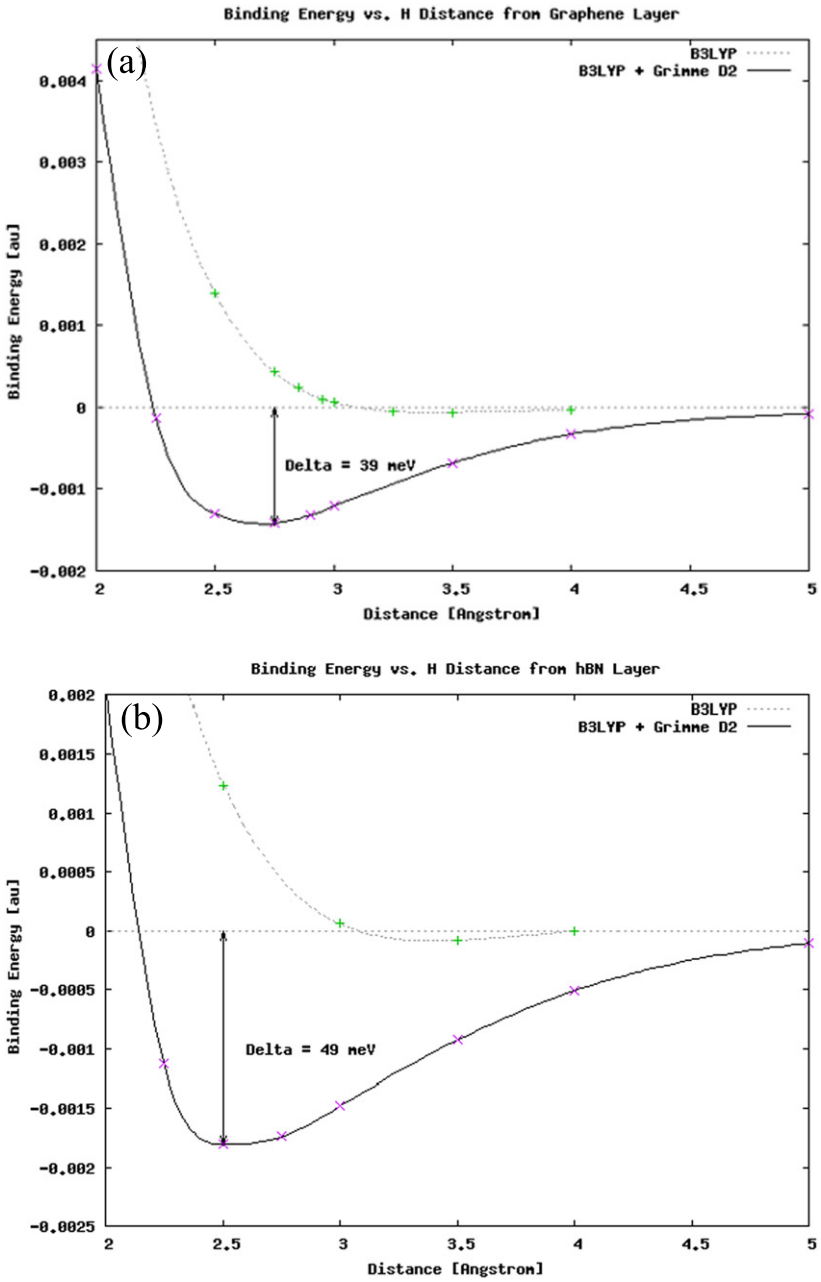

Figure 5. (a) Physisorption minimum of 0.039 eV for H on graphene at 2.75 A . The B3LYP and the B3LYP + Grimme's empirical dispersion binding energy curves are shown. (b). Physisorption minimum of 0.049 eV for H on hBN at 2.5 A.

compared to our results for the pristine graphene monolayer and to the results reported in [13].

Therefore, gas-phase and aqueous interaction potential curves are calculated as a function of the H_3O^+ hydronium ion distance perpendicular to the defect center. At a distance of 1 A above the center when the barrier starts to increase, the proton is released to pass through the center, leaving the H_2O molecule behind at 1 A (see figure 9). The results are shown in figure 10(a) for the gas phase and in figure 10(b) in the presence of water using again PCM.

As can be seen from figure 10, the gas-phase barrier for proton penetration at the defect site along the path described above is 1.05 eV, the lowest one obtained in our cluster models for proton transport through graphene. However, if the presence of water is taken into account within the polarizable continuum model, the barrier increases to 1.75 eV. This can be compared to 1.8 eV reported in [13] using VASP and modeling a water phase above and below graphene explicitely.

Finally, to check the selectivity of this defect site and complete the comparison with [13] which reports diffusion barriers of 1.8 eV for He and over 2.5 eV for H_2 for the hydroxyl-terminated site (as compared to 0.68 eV for proton penetration), barriers to helium and hydrogen molecule transfers through the oxygen-terminated defect site are calculated. We obtain

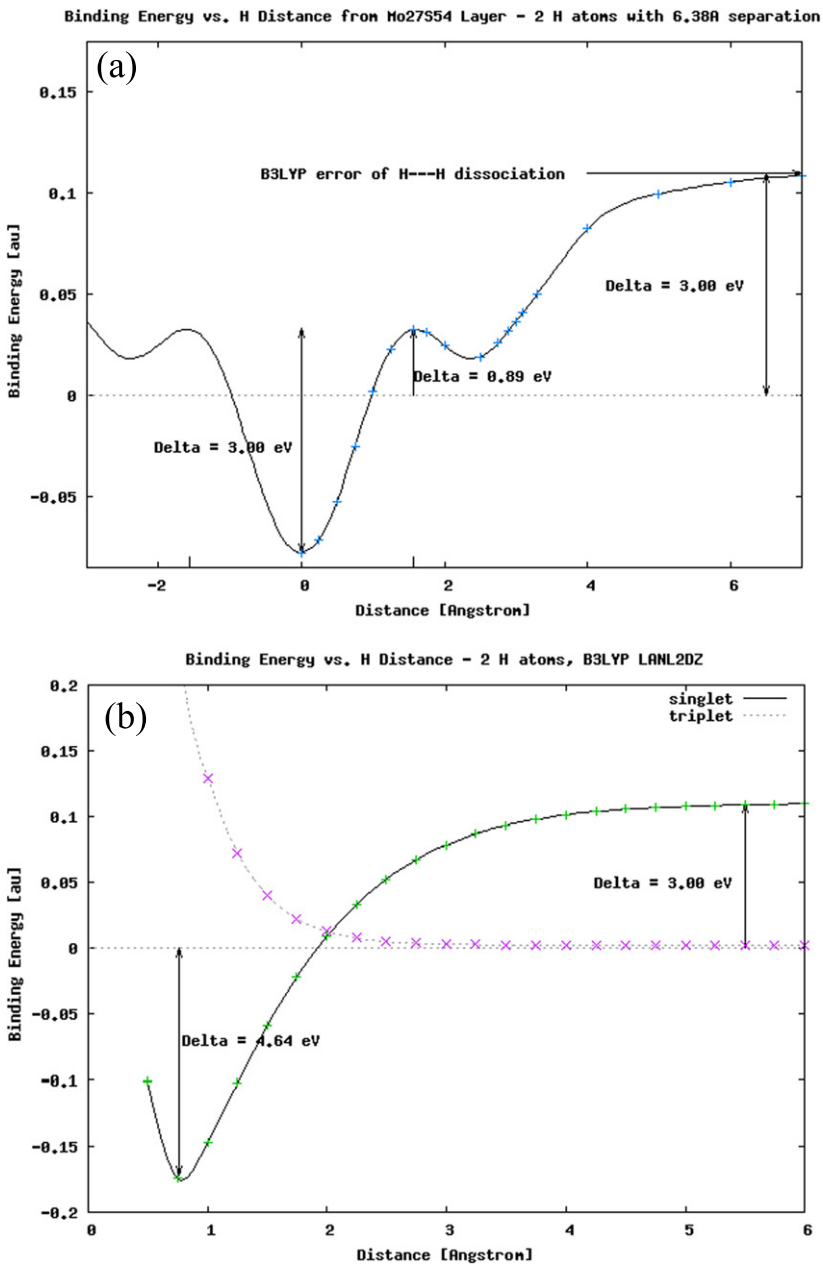

Figure 6. (a) Binding energy curve for 2 H atoms with constant separation of 6.38 A versus distance from the MoS_2 monolayer surface. For large D away from the surface, Δ approaches a value different from zero due to the improper dissociation of 2 open shell atoms in density functional theory. As shown in figure 6(b) which shows the singlet and triplet interaction curves for 2 H atoms this dissociation error obtained in B3LYP with the LANL2DZ basis is 3 eV.

5.64 eV for He and 8.11 eV for H_2 as gas-phase barriers (compared to 1.05 eV for the proton), clearly supporting the case for proton selectivity of this site.

4. Summary and conclusion

B3LYP cluster model calculations have been used to study the interaction potentials and gas-phase activation energies for protons and hydrogen atoms penetrating graphene, h-BN, phosphorene, silicene, and MoS_2 monolayers. The results indicate that only graphene and h-BN monolayers have the potential for membranes with high selective permeability. The interaction potentials for the MoS_2 monolayer are different from the results for the other materials in that they suggest that protons and H atoms become trapped between the outer *S* layers in the Mo plane, possibly explaining why no proton transport was detected for MoS_2, suggesting MoS_2 as a hydrogen storage material instead. For graphene, the calculated gas-phase and aqueous barriers of ~1.4 eV are too high to permit proton transfer through pristine graphene. Only h-BN has a low enough barrier (0.11 eV) to allow thermal protons to pass through. Contrary to other findings, platinum has a negligible effect on the barrier height in our model study. The smallest barrier for

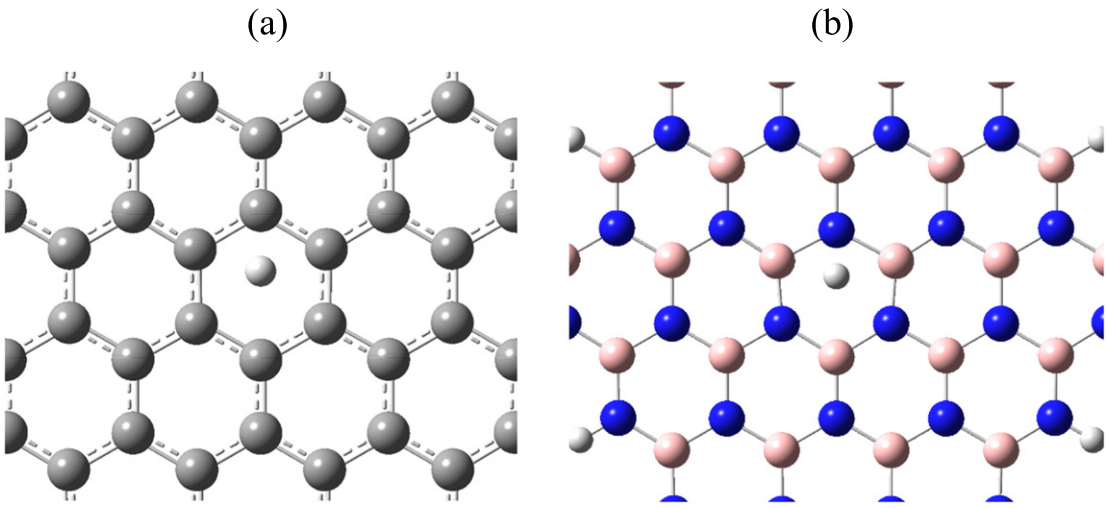

Figure 7. The proton penetration barrier is reduced to 1.38 eV for graphene (a) and to 0.11 eV for hBN (b) if the center hexagon and the in-plane position of the proton are allowed to relax. The strong ionic interaction in the hBN plane causes a larger disortion and larger off-center position of the proton. C atoms are gray, N atoms blue B atoms pink, the proton is white.

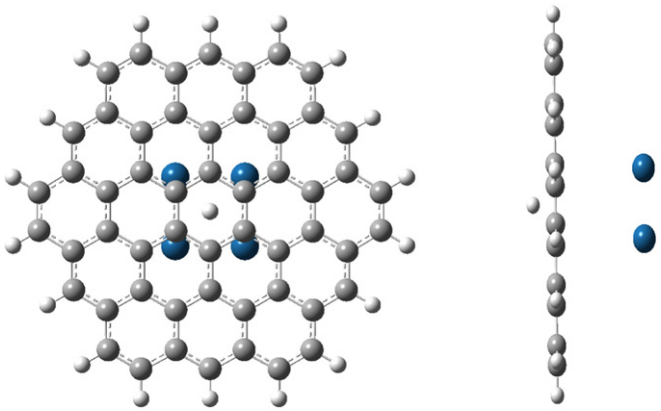

Figure 8. Model for the proton barrier in graphene in the presence of platinum. 4 Pt atoms (blue) in a square arrangement with side length 2.51 A are placed 4 A from the graphene cluster at the other side of the proton approach. The proton is shown 1 A above the center of central benzene ring.

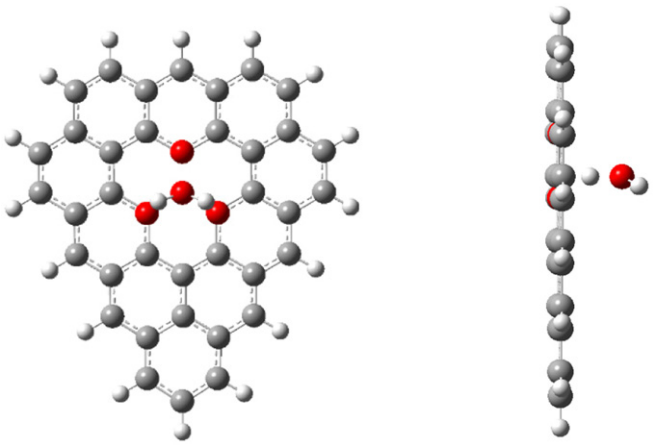

Figure 9. Top and side views of the quad-carbon vacancy site with three terminating oxygen atoms (in red) approached by a H_3O^+ hydronium ion.

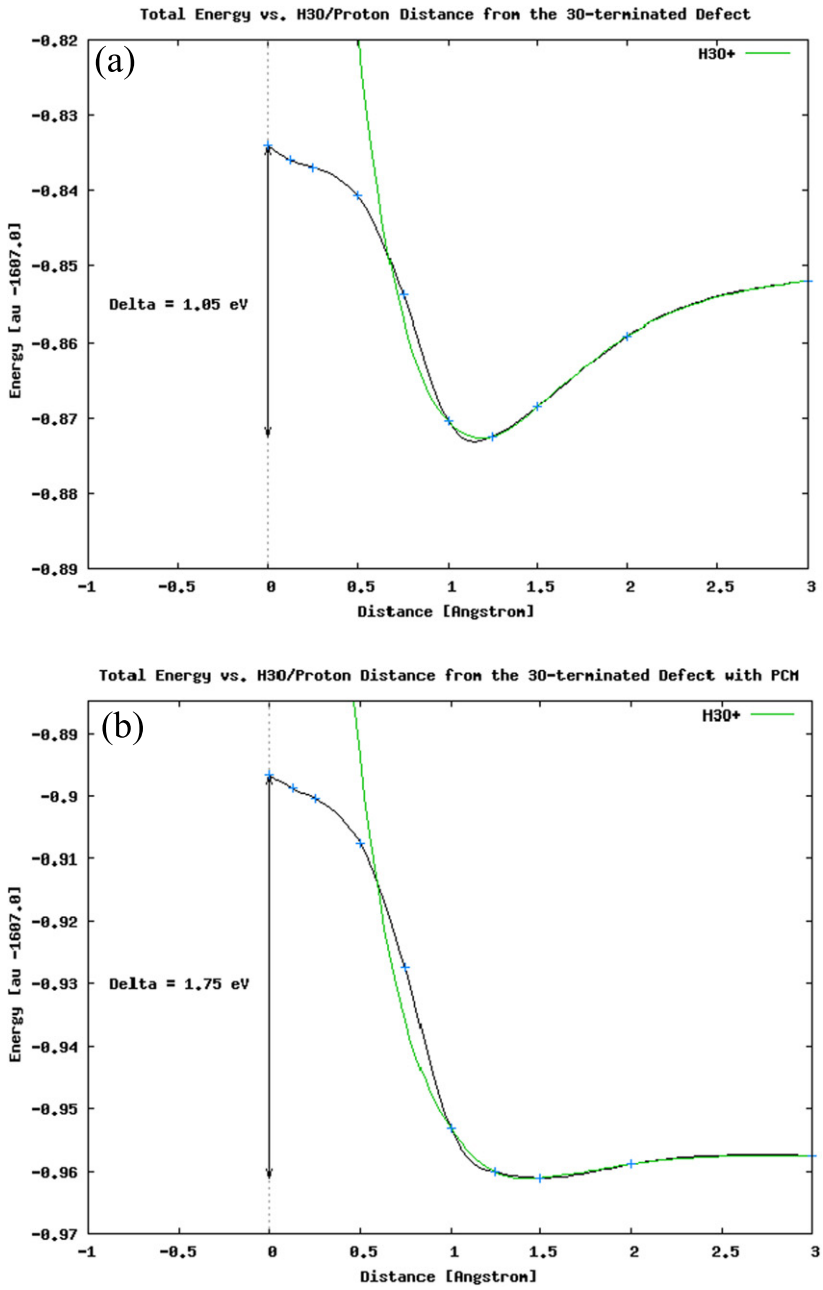

Figure 10. Gas-phase (a) and aqueous (b) interaction potential curves as a function of the H_3O^+ hydronium ion distance perpendicular to the defect center. At a distance of 1 A above the center when the barrier starts to increase, the proton is released to pass through the center, leaving the H_2O molecule behind at 1 A. The interaction potential curve if H_3O^+ would continue beyond 1 A is indicated in green.

proton diffusion through graphene (1.05 eV) is found for diffusion through an oxygen-terminated defect. Therefore, despite the inherent limitations of the cluster models, idealized chosen pathways, and the multitude of possible other pathways, it seems more likely that thermal protons can penetrate a monolayer of h-BN but not graphene and that defects in graphene are necessary to facilitate the proton transport.

Acknowledgments

Helpful discussions with Ranjit Pati, Gaoxue Wang who supplied geometries for phosphorene and MoS_2, Kevin Waters, and Dr Gowtham, Director of Research Computing, are gratefully acknowledged. The generous support with computer time by Michigan Tech's High Performance Computer Center is very much appreciated.

References

[1] Hu S *et al* 2014 *Nature* **516** 227–30
[2] Ornes S 2015 *PNAS* **112** 13128–30
[3] Vogt P, De Padova P, Quaresima C, Avila J, Frantzeskakis E, Asensio M C, Resta A, Ealet B and Le Lay G 2012 *Phys. Rev. Lett.* **108** 155501
[4] Liu H, Neal A T, Zhu Z, Tomanek D and Ye P D 2014 *ACS Nano* **8** 4033–41

[5] Ding Y and Wang Y 2015 *J. Phys. Chem.* C **119** 10610–22
[6] Ito A, Nakamura H and Takayama A 2008 *J. Phys. Soc. Japan* **77** 114602
[7] Boukhvalov D W, Knatsnelson M I and Lichtenstein A I 2008 *Phys. Rev.* B **77** 035427
[8] Eheman R, Krstic P S, Dadras J, Kent P R C and Jakowski J 2012 *Nanoscale Res. Lett.* **7** 198
[9] Miao M, Buongiorno Nardelli M, Wang Q and Liu Y 2013 *Phys. Chem. Chem. Phys.* 2013 **15** 16132–7
[10] Tsetseris L and Pantelides S T 2014 *Carbon* **67** 58–63
[11] Ma J, Michaelides A and Alfe D 2011 *J. Chem. Phys.* **134** 134701
[12] Wang W L and Kaxiras E 2010 *New J. Phys.* **12** 125012
[13] Achtyl J L *et al* 2015 *Nat. Commun.* **6** 6539
[14] Perdew J P 1991 *Electronic Structure of Solids '91* ed P Ziesche and H Eschrig (Berlin: Akademie Verlag) p 11
Perdew J P and Wang Y 1992 *Phys. Rev.* B **45** 13244–49
[15] Seel M and Bagus P 1981 *Phys. Rev.* B **23** 5464–71
[16] Frisch M J *et al* 2009 *Gaussian 09, Revision D.01* (Wallingford CT: Gaussian, Inc)
[17] Becke A D 1993 *J. Chem. Phys.* **98** 5648–52
[18] Lee C, Yang W and Parr R G 1988 *Phys. Rev.* B **37** 785–9
[19] Hay P J and Wadt W R 1985 *J. Chem. Phys.* **82** 270–83
[20] Kadantsev E and Hawrylak P 2012 *Solid State Commun.* **152** 909–13
[21] Kang J, Tongay S, Zhou J, Li J and Junqiao W J 2013 *Appl. Phys. Lett.* **102** 012111
[22] Spirko J A, Neiman M L, Oelker A M and Kamil K 2003 *Surf. Sci.* **542** 192–204
[23] Liang B and Andrews L 2002 *J. Phys. Chem.* A **106** 6945–51
[24] Zhang J, Soon J, Loh K, Yin J, Ding J, Sullivan M and Wu P 2007 *Nano Lett.* **7** 2370–2376
[25] Sierraaltaa A, Lisboaa O and Rodriguez L 2005 *J. Mol. Struct.* (*Theochem*) **729** 91–7
[26] Baehrends E J 2001 *Phys. Rev. Lett.* **87** 133004
[27] Bader R F W 1990 *Atoms in Molecules—A Quantum Theory* (Oxford: Oxford University Press)
[28] Tang W, Sanville E and Henkelman G 2009 *J. Phys. Condens. Matter* **21** 084204
[29] Yamamura S, Takata M and Sakata M 1997 *J. Phys. Chem. Solids* **58** 177–83
[30] Grimme S 2006 *J. Comput. Chem.* **27** 1787–99
[31] Tomasi J, Mennucci B and Cancès E 1999 *J. Mol. Struct.* (*Theochem*) **464** 211–26
[32] Kresse G and Furthmueller J 1996 *Phys. Rev.* B **54** 11169–86